Surface-element analysis of spatiotemporal stripe patterns formed by Ag and Sb coelectrodeposition

Yuko Nagamine and Masahiko Hara
Local Spatio-Temporal Functions Laboratory, Frontier Research System, RIKEN (The Institute of Physical and Chemical Research), 2-1 Hirosawa, Wako, Saitama 351-0198, Japan
(Received 21 October 2004; published 6 July 2005)

Various spatiotemporal patterns of light and dark stripes are formed in the Ag and Sb coelectrodeposition system. In this research, we report the results of the element analysis of three spatiotemporal stripe patterns using an electron probe (x-ray) microanalyzer. The results indicate that all the patterns have an O distribution reflecting the color configuration of the patterns, in addition to Ag and Sb distributions, which have been advocated as forming the patterns. It is suggested that O, as well as Ag and Sb, contributes to the formation of the patterns.

DOI: 10.1103/PhysRevE.72.016201 PACS number(s): 47.54.+r, 82.40.Ck, 82.40.Np, 81.15.Pq

I. INTRODUCTION

Systems with spatiotemporal functions under nonequilibrium conditions [1–4], exemplified by the Belousov-Zhabotinsky (BZ) reaction [1], have attracted considerable attention in recent materials science and engineering applications involving the field of computer programming such as analog computing [5]. Therefore, from an engineering viewpoint, controllability is important and the systems under tunable external parameters are suitable for practical applications because the experimental conditions of these systems can be reversibly and quickly adjusted. Examples of the spatiotemporal system are hydrodynamic Rayleigh-Bénard patterns formed by convection due to heat [6–8] or hydrodynamic patterns under shear flow [9], defect patterns of liquid crystals oriented under an electric field [10] or under a magnetic field [11], and adsorbate patterns on an electrode surface [12] or on a metal surface [13].

The Ag and Sb coelectrodeposited system [14] also has spatiotemporal functions under an external parameter, such as electric field. In this system, various spatiotemporal patterns are also formed on the electrode surface during electrodeposition, depending on the experimental conditions, e.g., a spiral pattern, a target pattern, a spot pattern, and a wave pattern, which all consist of light and dark parts. Furthermore, interestingly and uniquely, this system has spatiotemporal patterns made of metals, while most other systems have patterns made of soft materials. The light and dark parts have been reported to be rich in Ag and Sb using Auger spectroscopy, respectively [14,15]. In this study, in order to clarify the detailed element difference between light and dark parts in other elements in addition to Ag and Sb, we carried out surface element analysis for three spatiotemporal stripe patterns specified in terms of stripe wavelength and stripe velocity [16–18]. These three spatiotemporal stripe patterns (Fig. 1) can be found in the phase diagram obtained in our previous research [16].

II. EXPERIMENT

The electrolyte solution used for the coelectrodeposition of Ag and Sb consists of 0.15*M* $AgNO_3$, 0.036*M* $KSbOC_4H_4O_6 \cdot 3H_2O$, 0.21*M* $K_4Fe(CN)_6 \cdot 3H_2O$, 0.22*M* K_2CO_3, 1.5*M* KSCN, and 0.21*M* $KNaC_4H_4O_6 \cdot 4H_2O$ in distilled water. The used working electrode, which is electrodeposited using Ag and Sb, was a Au(111) thin film on mica (1×2 cm^2). The used counterelectrode was a 2×3 cm^2 Ag plate, part (1×2 cm^2) of which was removed from its center so that the pattern on the working electrode could be seen through the cut rectangular hole from outside of the container. During the electrodeposition, the pattern appearing on the working electrode surface was observed using an optical microscope with a zoom lens. The distance between the two

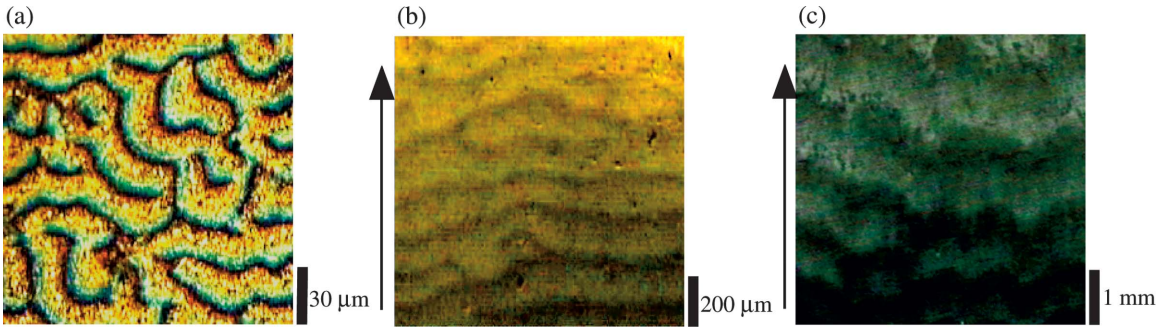

FIG. 1. (Color) Optical microscope images of three types of spatiotemporal stripe patterns. The arrows indicate the propagation directions of the stripes. (a) Complex labyrinthine structure. (b) Small wave structure. (c) Big wave structure.

electrodes was 1 cm. The electrodes were immersed vertically in an electrolyte solution. Due to the composition of the electrolyte solution, three types of spatiotemporal stripe patterns appear on the working electrode surface during the electrodeposition depending on the current density, as shown in the phase diagram of our previous paper [16]. The coelectrodeposition of Ag and Sb was carried out in the constant current mode at room temperature. A fresh working electrode was prepared for the electrodeposition at each specified constant current density. After confirming the emergence of the patterns, the applied current between the electrodes was turned off. Without applied current, the spatiotemporal patterns on the working electrode were immobilized on the spot. The working electrode was removed from the electrolyte solution and dried in air after rinsing in pure water.

The surface element analysis of the samples of the working electrodes was implemented using an electron probe (x-ray) microanalyzer (EPMA), which can disperse characteristic x-rays emitted from the sample after incidence of the electron beam, in terms of wavelength in five channels by crystal lattices and the detected wavelength range of each channel could be changed by choosing a crystal lattice among the two crystal lattices equipped in each channel. The EPMA has various kinds of crystal lattice, ten in total, so that five spectra in different wavelength ranges of the characteristic x-ray can be obtained at the same time. In the spectra, the intensity peaks due to elements that make up the sample appear. In this research, the ranges which cover the peaks of the elements included in the electrolyte solution for electrodeposition were chosen. The intensities of the peaks in these detected spectra can be finally converted to the atomic percents of the elements on the measurement area of the sample. Furthermore, on fixing a crystal lattice in a certain position where one peak in these characteristic x-ray spectra can be detected and on carrying out a sample scan of the electron beam by moving the sample stage, an intensity map can be created for the scanned sample area. This intensity map can also be converted into an element map in atomic percent whose element contributes to the peak. In this experiment, the maps are made up of 300×300 pixels. In the element map, the spatial resolution is the diameter of the electron beam of the EPMA scanning area. The diameter of the electron beam is determined by one pixel size of an element map when one pixel size is larger than 1 μm^2, while the diameter is fixed to 1 μm when one pixel size is smaller than 1 μm^2 because the limit of the diameter of the electron beam is approximately 1 μm. For example, the spatial resolution is 4 μm for the element maps of the big wave structure (Fig. 3), 3 μm for those of the small wave structure (Fig. 5), and 1 μm for those of the complex labyrinthine structure (Fig. 7). For the conversion of the intensity of the characteristic x-ray peak to the atomic percent of the element, well-known empirical calibration factors of standard samples for the respective elements were used. The electron beam intensity used in this study was 20.0 kV.

III. RESULTS

Figures 1(a)–1(c) show optical microscope images of the three spatiotemporal stripe patterns called the complex labyrinthine structure, the small wave structure and the big wave structure, respectively. The stripe wavelength of the complex labyrinthine structure [Fig. 1(a)] is on the order of 10 μm. This pattern moves isotropically at a speed of ~ 1 μm/s, maintaining the isotropy of the pattern configuration. The shape of the complex labyrinthine structure is very similar to that of the complex pattern in a periodically forced surface reaction-diffusion system [19,20], although the complex labyrinthine structure in the Ag and Sb coelectrodeposition system emerges under direct current. The stripe of the small wave structure [Fig. 1(b)] lies in the horizontal direction. This stripe wavelength is on the order of 100 μm. This small wave structure propagates vertically along the electrode surface at a speed of ~ 10 μm/s. The line direction of the big wave structure [Fig. 1(c)] is also horizontal, and its wavelength is on the order of 1 mm. This wave structure, as well as the small wave structure, moves upwards along the electrode surface at a rate of $\sim 100 \mu$m/s. Namely, these three spatiotemporal stripe patterns have a difference of a few digits in stripe wavelength. The big wave structure has a unique characteristic compared with the other structures; it moves toward the top of the electrode destroying the complex labyrinthine structure or the small wave structure, which is formed on the electrode surface [16].

A. Characteristic x-ray spectroscopy

Figure 2 shows the representative characteristic x-ray spectra of the complex labyrinthine structure in five channels. The area with a diameter of 300 μm was measured by setting a diameter of the electron beam of the EPMA for 300 μm. These spectra show the average spectra of the complex labyrinthine structure because the measured area includes more than ten stripes of the complex labyrinthine structure. In addition to the peaks of Ag and Sb, the peaks of O, C, S, and K were detected. The peaks of these six elements were observed in all three spatiotemporal stripe patterns. This indicates that the other four elements also contribute to the pattern with Ag and Sb.

B. Element map analysis for big wave structure

Figure 3 shows the maps of the six elements for the area of the big wave structure shown in the optical microscope image in Fig. 3(a). All the maps present a pattern by the element distribution reflecting the pattern configuration of the big wave structure shown in Fig. 3(a). A comparison of the Ag map with the optical microscope image reveals that the atomic percent of Ag in the light-stripe area is higher than that in the dark-stripe area while a comparison of Sb, O, C, S, and K maps shows that the atomic percents of these elements in the dark-stripe area are higher than those in the light-stripe area. The average atomic percents for the entire area of element maps are shown in Table I. It is notable that the average atomic percents of O (11 at. %) and C (11 at.%) are higher than that of Sb (6.8 at. %) among five elements whose atomic percents are higher in the dark-stripe area. Table I also shows the average element atomic percents for the light- and dark-stripe areas of the big wave structure calculated from the respective maps. In addition, the ratios of

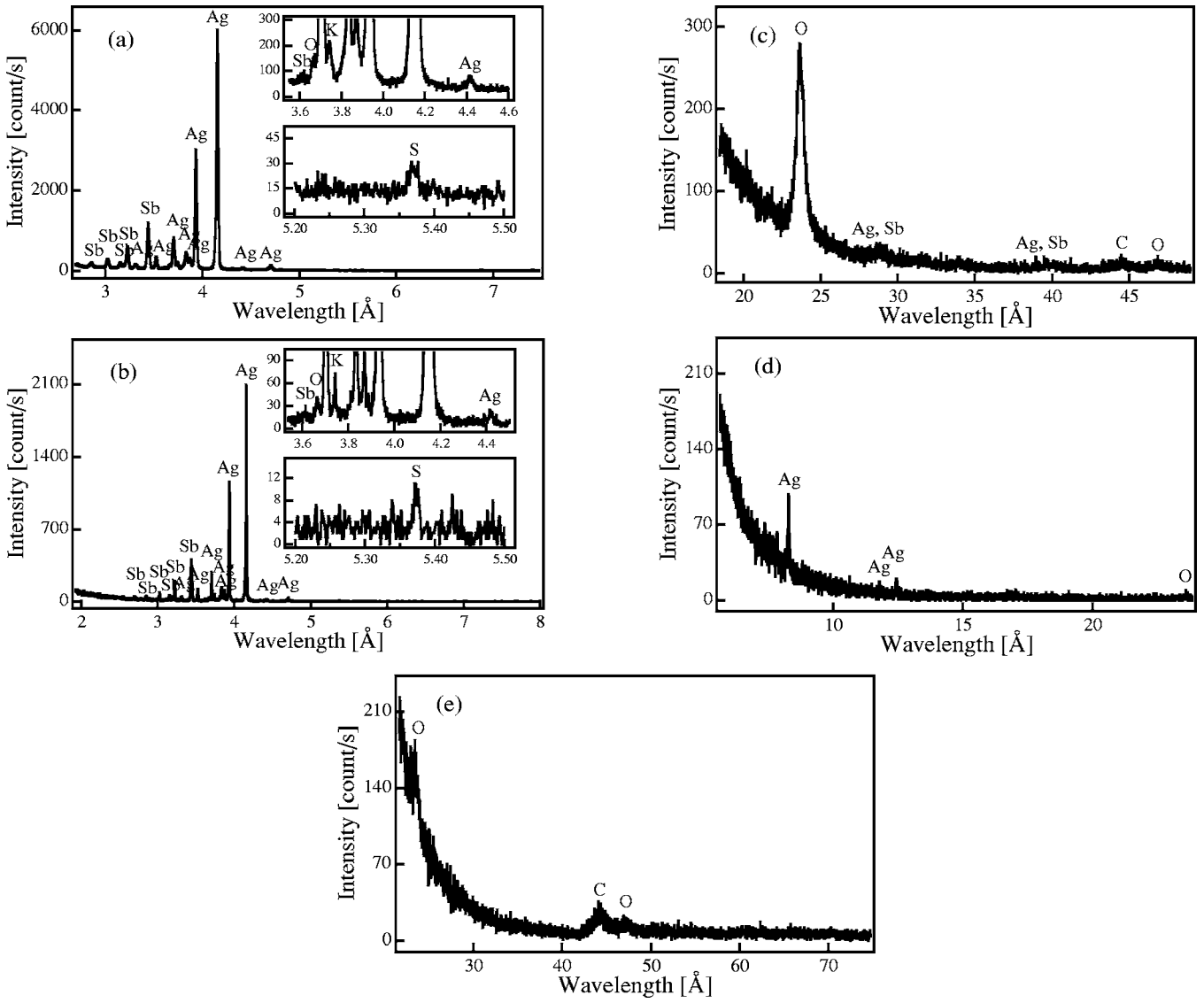

FIG. 2. Characteristic x-ray spectra for complex labyrinthine structure obtained by five channels at the same time. The diameter of the measurement area is 300 μm. (a) Channel 1 (2.7–7.5 Å). (b) Channel 2 (1.9–8.0 Å). (c) Channel 3 (18–49 Å). (d) Channel 4 (5.6–24 Å). (e) Channel 5 (22–75 Å).

the respective atomic percent in the dark-stripe area to that in the light-stripe area are shown in Table I. The ratio indicates the difference in atomic percent between the dark- and light-stripe areas and a higher ratio indicates that the atomic percents between dark and light stripes change more substantially. The results reveal that the ratio of Sb atomic percent is the lowest among those of the five elements, whose atomic percents are higher in the dark-stripe area. Namely, O and C are higher than Sb both in terms of the average atomic percent for the entire area of the element map and in terms of the ratio of the atomic percent in the dark-stripe area to that in the light-stripe area.

Furthermore, the element maps of the big wave structure under a high magnification are shown in Fig. 4. The optical microscope image [Fig. 4(a)] shows that there are many crystals in the dark-stripe area [18]. In addition to crystals, the C- and K-rich part in the dark-stripe area can be locally observed on the element maps.

Local characteristic x-ray spectroscopy of two distinctive points in the dark-stripe area, namely the crystal part and the C- and K-rich part, was implemented in the measurement area with a diameter of 1 μm. From the peak intensities in the obtained spectra, the elements' atomic percents in the measurement area were directly calculated. Table II shows the results for the two points. The data for the crystal part reveals that the part is mainly composed of Ag (81 at. %) and suggests that these crystals are Ag crystals. The C- and K-rich part is chiefly composed of three elements, Ag (17 at. %), C (50 at. %), and K (16 at. %). In this part, the atomic percents of C and K are significantly higher than the average C and K atomic percents (11 and 3.4 at. %, respectively) for the area of the element maps (Table I), respectively. From this result, it is expected that this part might be formed by the aggregation of the salt involved in the electrolyte solution for electrodeposition.

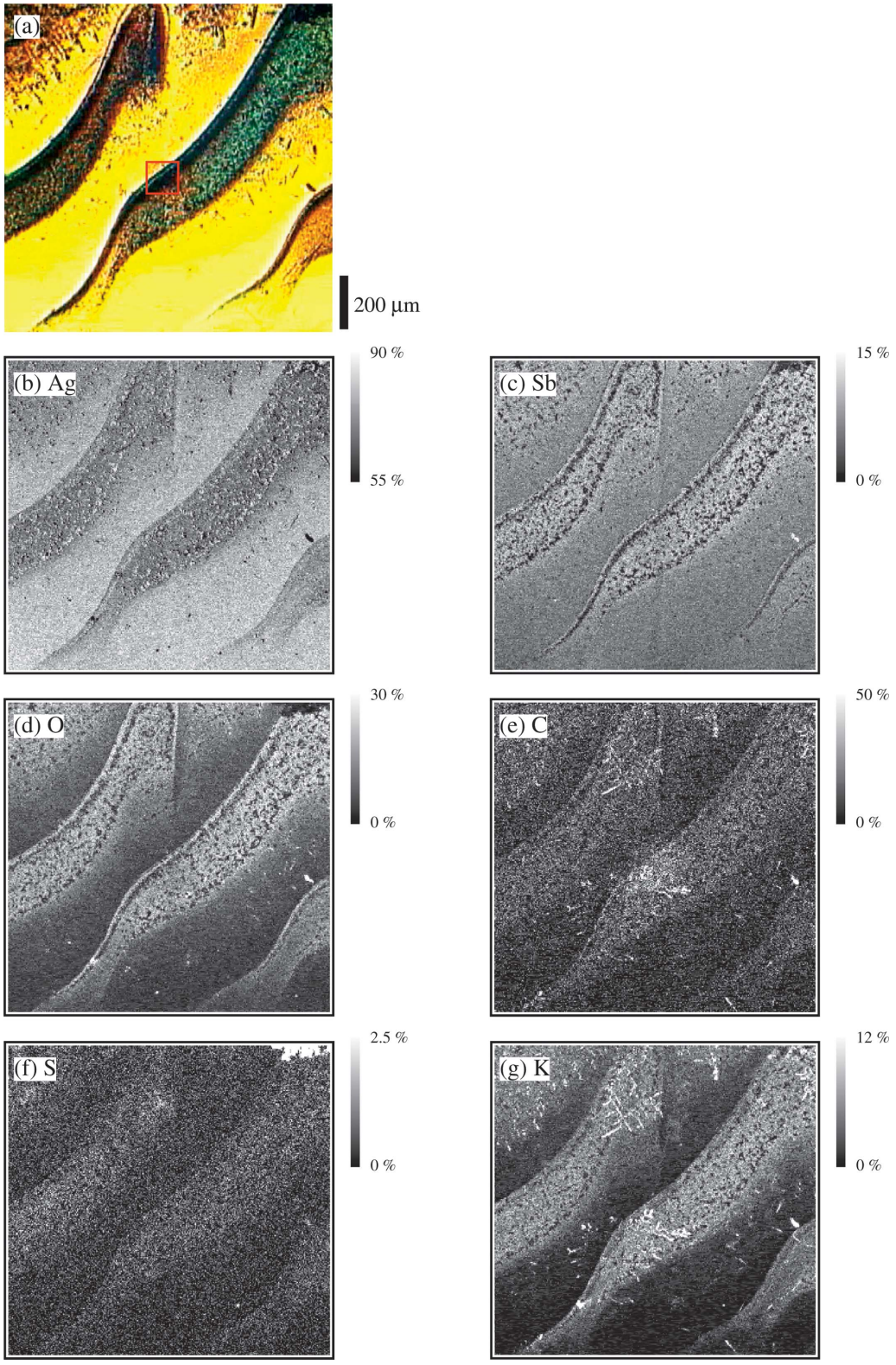

FIG. 3. (Color) Optical microscope image of big wave structure [(a)] and maps of six elements for area shown in (a) [(b) Ag map, (c) Sb map, (d) O map, (e) C map, (f) S map, and (g) K map]. The color bars on the right-hand side of the element maps indicate the respective element atomic percents.

C. Element map analysis of small wave structure

Figure 5 shows the maps of the six elements for the small wave structure shown by the optical microscope image in Fig. 5(a). In the small wave structure, the maps of the four elements [Figs. 5(b), 5(d), 5(f), and 5(g)] except for Sb and C present a clear pattern of the element distribution as well as

TABLE I. Average element atomic percents for the entire area of respective element maps in big wave structure, and average element atomic percents of light- and dark-stripe areas calculated by element maps. The ratios of the atomic percent of respective elements in the dark stripe to that in the light stripe are noted.

	Average (at. %)	Light stripe (at. %)	Dark stripe (at. %)	Ratio
Ag	74	81	69	0.85
Sb	6.8	5.3	9.7	1.8
O	11	7.1	19	2.7
C	11	5.9	26	4.4
S	0.38	0.21	1.4	6.7
K	3.4	2.1	7.5	3.6

the pattern color configuration shown in Fig. 5(a). In the Sb and C maps [Figs. 5(c) and 5(e)] and (e)), the patterns could scarcely be seen. A comparison of the maps of the four elements, which have a clear pattern as shown in the optical microscope image of Fig. 5(a), reveals that the Ag atomic percent in the light-stripe area is higher than that in the dark-stripe area and the atomic percents of the O, S, and K in the dark-stripe area are higher than those in the light-stripe area. The average atomic percents of the respective element maps for the entire area are shown in Table III. In the small wave structure as well as the big wave structure, the atomic percent of O (8.1 at. %) is also much higher than that of Sb (4.4 at. %). In Table III the average element atomic percents for the light- and dark-stripe areas calculated using the respective element maps are also shown. The results reveal that the ratio of O atomic percent in the dark-stripe area to that in the light-stripe area is higher than the corresponding Sb atomic percent ratio.

Furthermore, in the small wave structure, the element maps of the small wave structure under a high magnification are also depicted in Fig. 6. The area where the element map analysis was implemented is shown in the optical microscope image in Fig. 6(a). Figure 6(a) also shows that there are many crystals in the dark-stripe area [18], as well as the big wave structure. In addition to crystals, the C-rich part in the dark-stripe area can also be locally observed on the element maps.

The local characteristic x-ray spectroscopy of the two peculiar parts in the dark-stripe area, for the crystal part, and the local C-rich part was implemented. The investigation was carried out in a measurement area with a diameter of 1 μm. Table IV shows the results for two such points. The data of the crystal part reveals that the part is mainly composed of Ag (83 at. %) and it suggests that these crystals might also be Ag crystals. The local C-rich part is chiefly composed of C (85 at. %). This area might also be formed by the aggregation of salt as well as the big wave structure mentioned above.

D. Element map analysis for complex labyrinthine structure

Figure 7 shows the maps of the six elements for the area of the complex labyrinthine structure shown in the optical microscope image of Fig. 7(a). In the optical microscope image, the crystals can already be recognized along with the pattern configuration of the complex labyrinthine structure because of the small size of the structure. The crystals in the complex labyrinthine structure are in the light-stripe area, not in the dark-stripe area where the crystals in the big and small wave structures exist [18]. In addition to crystals, the C- and K-rich parts in the complex labyrinthine structure area can be observed in several local places on the element maps.

In this structure, the maps of the five elements except for C show a pattern of the element distribution as well as the pattern color configuration shown in Fig. 7(a). Comparing the respective five element maps with the optical microscope image shown in Fig. 7(a), it is revealed that the atomic percents of Ag and S are higher in the light-stripe area than in the dark-stripe area, while the atomic percents of Sb, O, and K are increased in the dark-stripe area. From these results, it is found that the S distribution is more distinct than those in the small and big wave structures; S has a more concentrated distribution in the light-stripe area than in the dark-stripe area in the complex labyrinthine structure, whereas S has a more dense distribution in the dark-stripe area in the big and small wave structures. However, the S distribution is coincident with the crystal distribution in all the patterns, although the atomic percent of S is small for the total amount.

The average element atomic percents for the entire area of the respective element maps are shown in Table V. In this structure, the average atomic percent of O (11 at. %) is also higher than that of Sb (8.8 at. %). Table V also shows the average element atomic percents of the light- and dark-stripe areas calculated by the respective element maps and the ratio of the O atomic percent in the dark-stripe area to that in the light-stripe area is also higher than the corresponding Sb atomic percent ratio.

In Table V the atomic percents for the crystal part and the C- and K-rich part are summarized. These values were obtained using the characteristic x-ray spectra locally carried out in the measurement area with a diameter of 1 μm. The element atomic percents of the crystal part also reveal that the part is mainly composed of Ag (67 at. %), which suggests that these crystals might be Ag crystals in the complex labyrinthine structure as well as in the small and big wave structures. The atomic percents of the C- and K-rich part show that this area is also composed of high amounts of C. This area of this structure might be also formed by the aggregation of salt.

IV. DISCUSSION

The results indicate that, commonly in all patterns, the light-stripe area contains more Ag than the dark-stripe area and the dark-stripe area tends to contain more Sb, O, and K than the light-stripe area. These three elements might be strongly associated with the reaction that forms the dark stripes in the three patterns.

Moreover, the results revealed that the crystals, which selectively exist in the light- or dark-stripe area, are composed mostly of Ag and scarcely of Sb in all the patterns, and the difference in the atomic percent of the elements between the

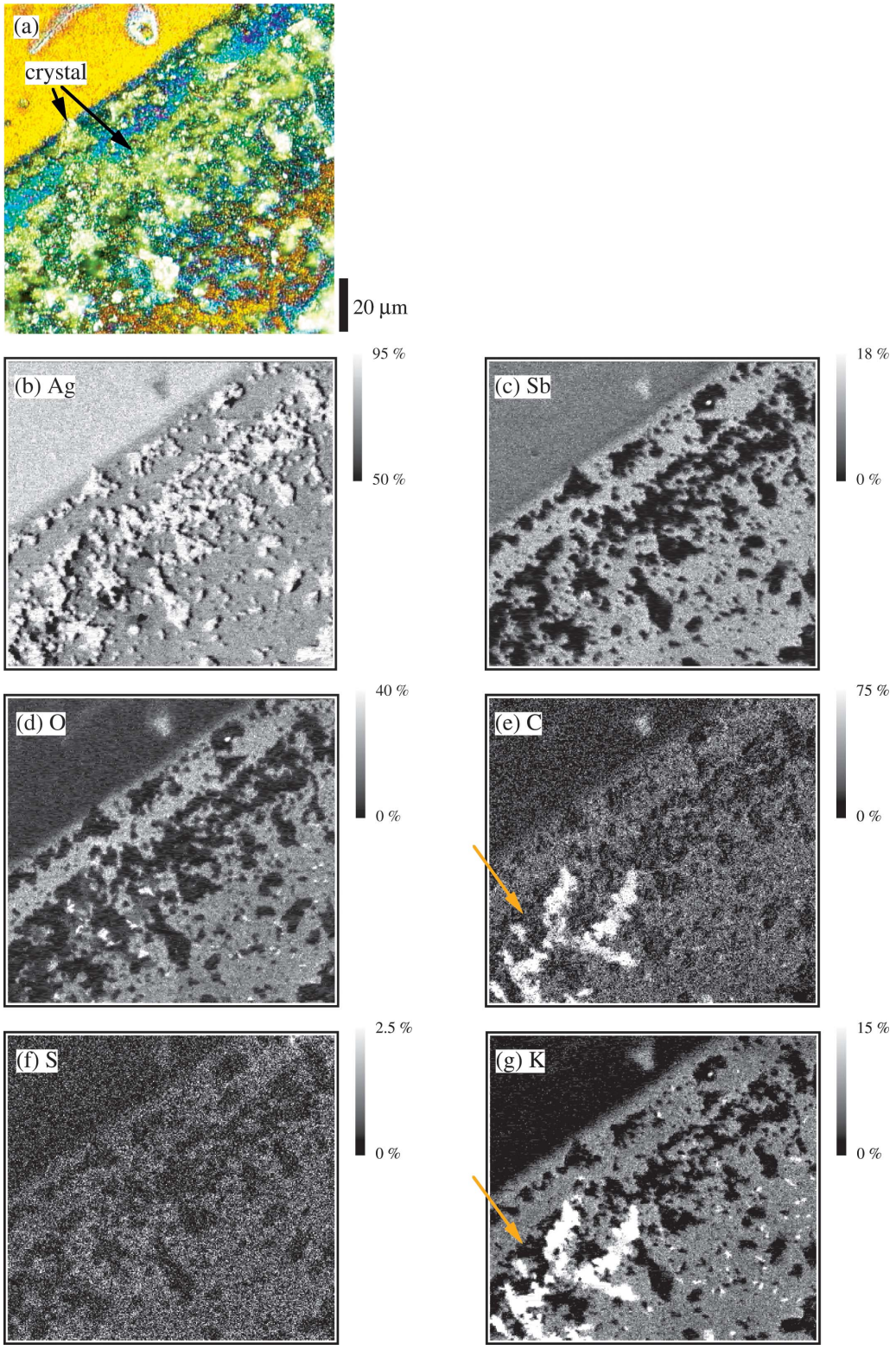

FIG. 4. (Color) Optical microscope image of big wave structure under high magnification [(a)] and maps of six elements for area shown in (a) [(b) Ag map, (c) Sb map, (d) O map, (e) C map, (f) S map, and (g) K map]. This area corresponds to the area shown by the red rectangle in Fig. 3(a). The color bars on the right-hand side of the respective element maps indicate the element atomic percents. The yellow arrows in (e) and (g) show the C- and K-rich part.

crystals and the matrix including the light-stripe and the dark-stripe areas except for the crystals is marked. The average atomic percents for the matrix are very close to the average for the entire area in the element maps. Such a difference might indicate the phase separation of Ag from the matrix [18].

TABLE II. Element atomic percents for two local areas in the dark-stripe area in big wave structure investigated in a measurement area with a diameter of 1 μm. The element atomic percents for the crystal part and the C- and K-rich part on the dark-stripe area are shown.

	Crystal part (at. %)	C- and K-rich part (at. %)
Ag	81	17
Sb	0.35	2.8
O	3.2	2.9
C	15	50
S	0.33	0.33
K	0.75	16

A. Contribution of O atoms to pattern formation

Furthermore, the results clarify that more O atoms are contained in all three spatiotemporal patterns than Sb atoms and, in addition, the ratio of the O atomic percent in the dark stripe to that in the light stripe is larger than the corresponding Sb atomic percent ratio in all the patterns, which reveals that the number of O atoms changes among stripes more substantially than the number of Sb atoms in all the patterns. The results suggest that O more weighs with a composition of the pattern, particularly, of the dark stripe, than Sb, in all the spatiotemporal patterns.

As an origin of O, two models are proposed. One is that O originates from the chemical compounds included in the electrolyte solution for the electrodeposition. In the electrolyte solution, any O included in the chemical compounds combines with C or N. Therefore the O distribution ought to be coincident with the N distribution or C distribution in the element map analysis results. However, N is not detected in all the characteristic x-ray spectra for the three spatiotemporal patterns as shown in Fig. 2 and the C distribution does not always coincide with the O distribution in the element maps. Although the C distribution coincides with the O distribution in the big wave structure, the C distribution does not coincide with the O distribution in the small wave structure and the complex labyrinthine structure. In the big wave structure, the ratio of the O atomic percent to C atomic percent in the dark-stripe area in which stripes containing O and C become more distinct, as shown in Table I, O/C=19/26, is lower than the ratios of the number of O atoms to that of C atoms in all chemical compounds involving O and C in the electrolyte solution for the electrodeposition (7/4 in $KSbOC_4H_4O_6$, 3/1 in K_2CO_3, and 6/4 in $KNaC_4H_4O_6$). The ratio of O to C in the big wave structure is different from that in the electrolyte solution.

As another model, it is suggested that O originates from metal oxidation, namely, Ag or Sb oxidation during electrodeposition. In the element maps of the three spatiotemporal patterns, Ag distributions are always opposite to O distributions, while Sb distributions are similar to O distributions. Therefore it is speculated that there is a higher possibility of Sb oxidation than of Ag oxidation. In fact, according to the literature [21], Sb is oxidized at approximately −670 mV vs SHE (standard hydrogen electrode). The value is within the potential range at which the three spatiotemporal patterns are formed; this range is from −650 to −750 mV vs SHE, from our previous investigation [17]. The oxidation of Sb is represented in the electrochemical reaction formula as follows [21].

TABLE III. Average element atomic percents for the entire area of respective element maps in a small wave structure and average element atomic percents for light- and dark-stripe areas calculated by element maps. The ratios of the atomic percent of respective elements in the dark stripe to that in the light stripe are calculated.

	Average (at. %)	Light stripe (at. %)	Dark stripe (at. %)	Ratio
Ag	75	80	72	0.9
Sb	4.4	4.4	4.4	1.0
O	8.1	5.8	11	1.9
C	4.6	4.6	4.6	1.0
S	0.82	0.41	1.6	3.9
K	1.9	0.98	2.8	2.9

$$Sb + 4OH^- \rightarrow SbO_2^- + 2H_2O + 3e^-, \quad E^\circ = -670 \text{ mV vs SHE}. \tag{1}$$

This reaction proceeds to the right-hand side in an alkaline solution. Actually, the electrolyte solution for coelectrodeposition in our experiment is an alkaline solution and this reaction could proceed in our system. This reaction indicates that Sb is redissolved in the electrolyte solution as an ion of antimony dioxide. Therefore, around this potential, the adsorption and desorption of Sb to the electrode surface might coexist. Such a bistable system by the adsorption and desorption of Sb might form a spatiotemporal pattern [22]. The state analysis of Ag and Sb will be investigated in order to clarify whether this expectation is valid in the near future. At present, from this potential value, the latter case is considered to be plausible.

However, with only this bistability, travelling waves such

TABLE IV. Element atomic percents for two local areas in the dark stripe in a small wave structure detected in a measurement area with a diameter of 1 μm. The element atomic percents for the crystal part and C-rich part on the dark-stripe area are shown.

	Crystal part (at. %)	C-rich part (at. %)
Ag	83	11
Sb	1.5	0.59
O	2.9	2.1
C	10	85
S	0.80	0.39
K	1.4	0.94

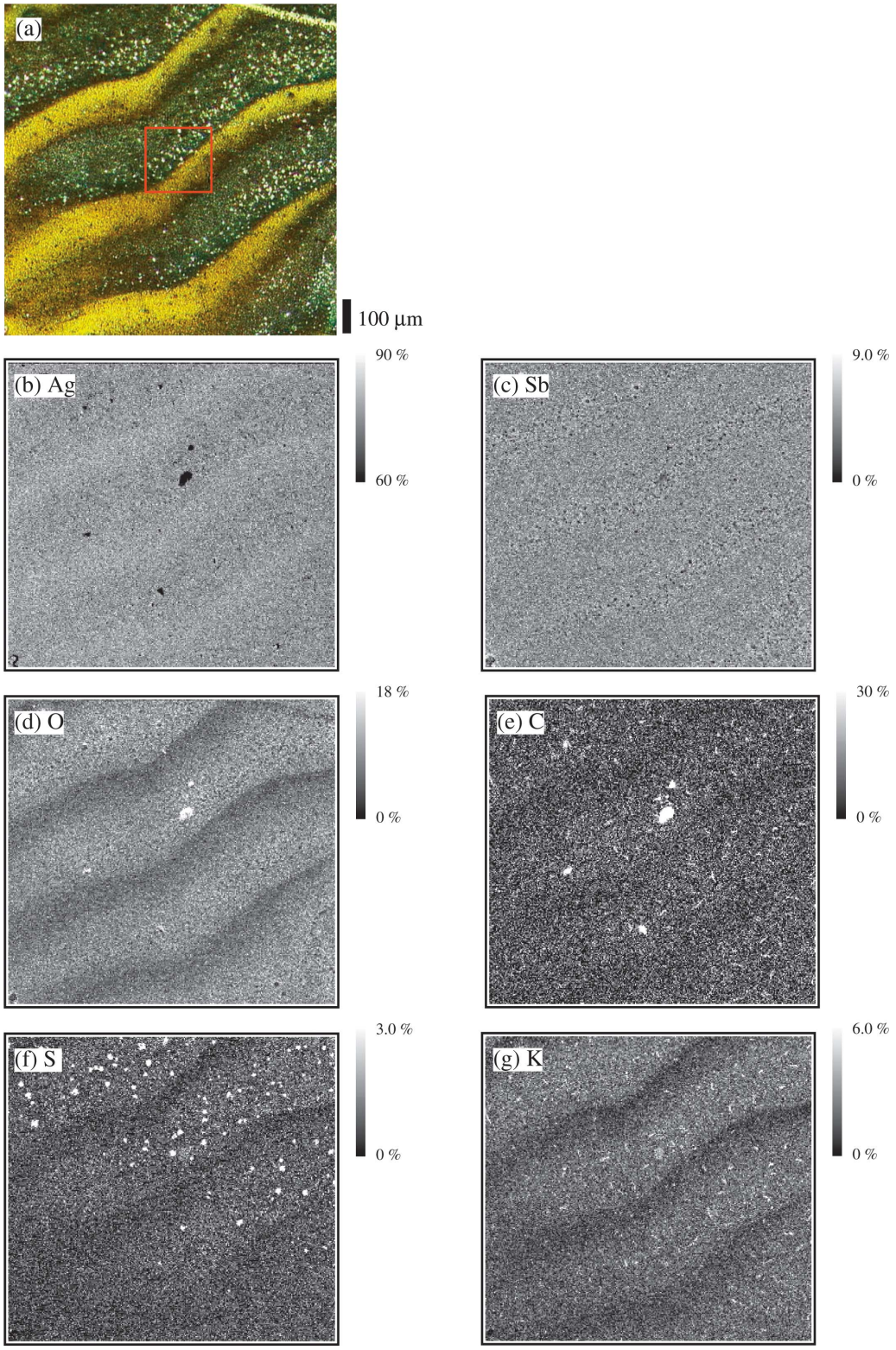

FIG. 5. (Color) Optical microscope image of small wave structure [(a)] and maps of six elements for area shown in (a) [(b) Ag map, (c) Sb map, (d) O map, (e) C map, (f) S map, and (g) K map]. The color bars on the right-hand side of the element maps indicate the respective element atomic percents.

as these spatiotemporal stripe patterns in this system could not be explained. Additional physical factors may be responsible for the propagation of the stripe. As a physical factor, the convection emerging on the electrode surface is suggested [23–25]. Generally, the convection along the electrode surface is formed in the vicinity of the electrodeposited electrode and the convection flows from the bottom to the top of the electrode [23]. This convection is formed by the buoy-

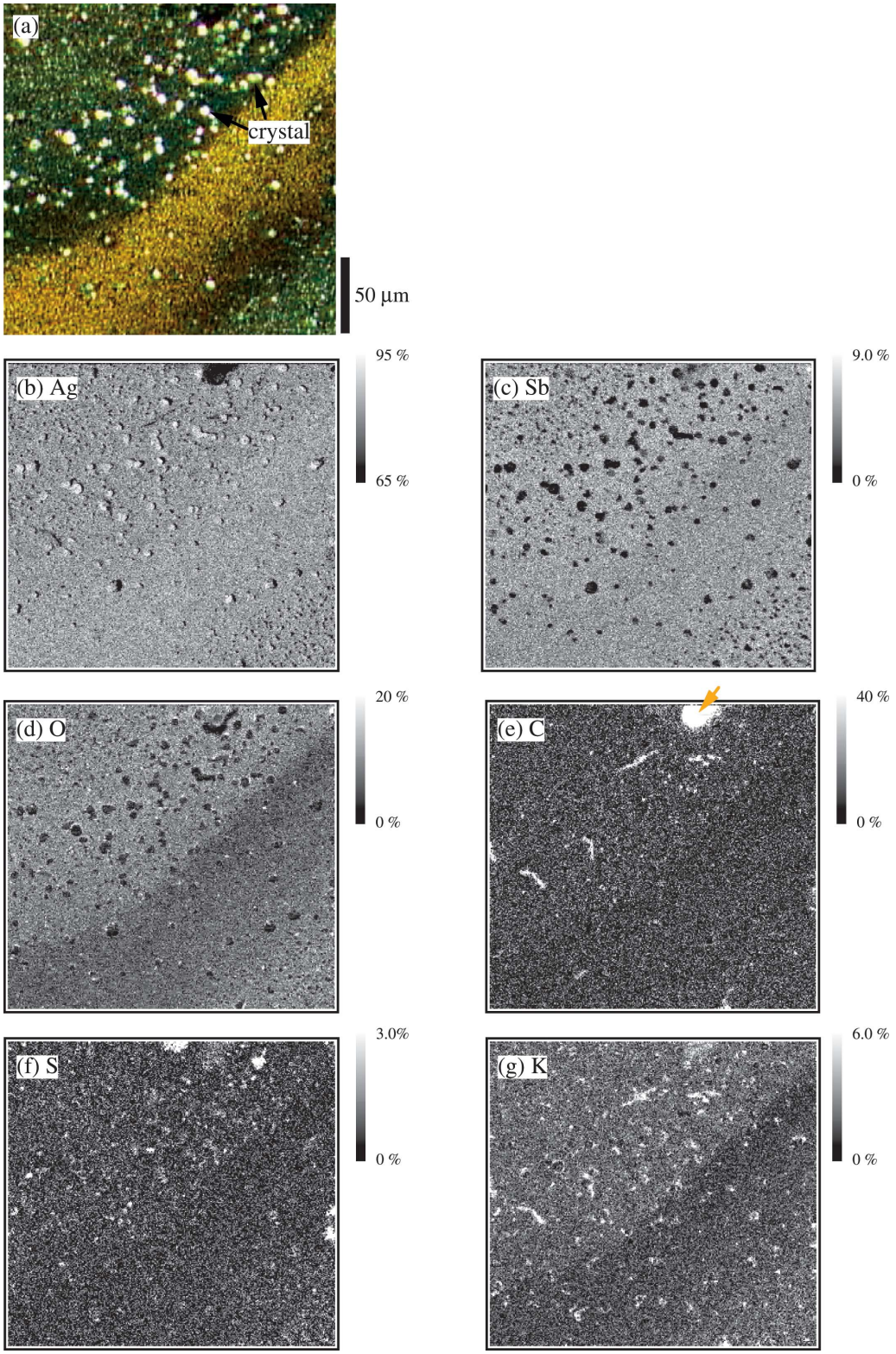

FIG. 6. (Color) Optical microscope image of the small wave structure under high magnification [(a)] and maps of six elements for area shown in (a) [(b) Ag map, (c) Sb map, (d) O map, (e) C map, (f) S map, and (g) K map]. This area corresponds to the area shown by the red rectangle in Fig. 5(a). The color bars on the right-hand side of the element maps indicate the respective element atomic percents. The yellow arrow in (e) shows the C-rich part.

ancy effect which results from the metal ion concentration difference between the electrolyte solution around the electrodeposited electrode surface and the bulk electrolyte solution. The metal ion concentration around the electrodeposited electrode is less dense because the metal ions in the vicinity of the electrode adsorb onto the electrode surface, which is

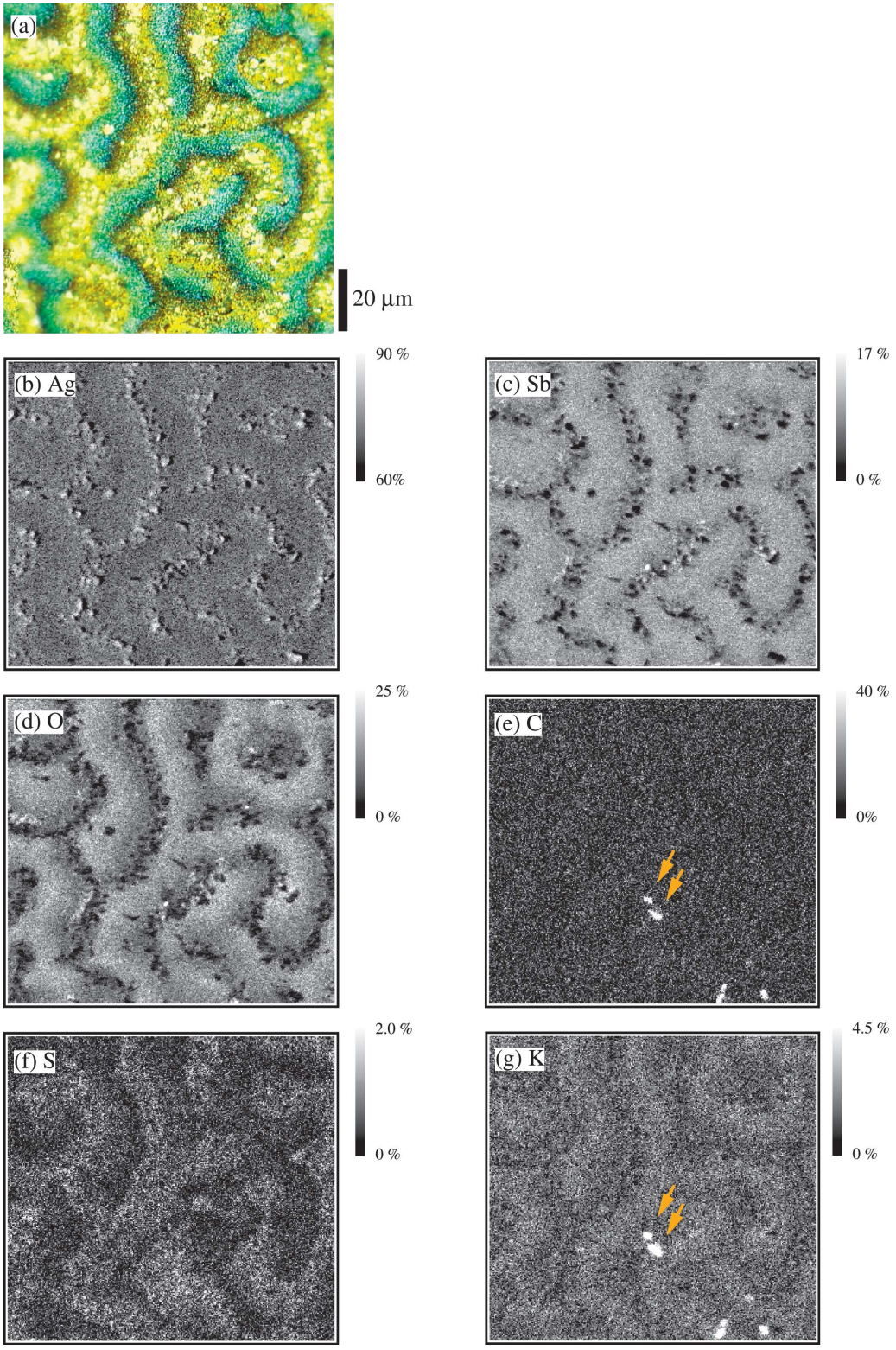

FIG. 7. (Color) Optical microscope image of complex labyrinthine structure [(a)] and maps of six elements for the area shown in (a) [(b) Ag map, (c) Sb map, (d) O map, (e) C map, (f) S map, and (g) K map]. The color bars on the right-hand side of the element maps indicate the respective element atomic percents. The yellow arrows in (e) and (g) show two points of the C- and K-rich part.

forced by the current applied between electrodes for electrodeposition. In this Ag and Sb electrodeposition system, such convection is considered to emerge on a Ag and Sb coelectrodeposited electrode surface where spatiotemporal stripe patterns exist, in the same mechanism. It is expected that, especially, the small and big wave structures' formation is strongly dependent on such convection from the anisotropic shape and movement of the patterns.

TABLE V. Average element atomic percents for the entire area of respective element maps in complex labyrinthine structure and average element atomic percents for light- and dark-stripe areas calculated by element maps. The ratios of the atomic percent of respective elements in the dark stripe to that in the light stripe are noted. The element atomic percents for the two local areas, the crystal part, and the C- and K-rich part, are represented, which were examined in the measurement area with a diameter of 1 μm.

	Average (at. %)	Light stripe (at. %)	Dark stripe (at. %)	Ratio	Crystal part (at. %)	C- and K-rich part (at. %)
Ag	71	76	68	0.89	67	48
Sb	8.8	6.3	11	1.7	1.4	6.6
O	11	7.7	16	2.1	3.5	6.2
C	8.0	8.0	8.0	1.0	17	31
S	0.57	1.1	0.22	0.2	0.66	0.75
K	1.6	0.64	2.1	3.3	0.85	6.1

B. Distribution of O atoms and propagation direction of pattern

Moreover, the element distributions on the red broken lines drawn in Figs. 8(a), 9(a), and 10(a), which were plotted using the element maps shown in Figs. 3, 5, and 7, respectively, were investigated. The atom distributions of O on the red broken lines [Figs. 8(d), 9(d), and 10(d)] show a periodic asymmetric shape like a sawtooth, and such a shape asymmetry of O is clearer than that of Sb [Figs. 8(c), 9(c), and 10(c)]. In the big wave structure, a comparison of this asymmetric shape in Fig. 8(d) with the optical microscope image in Fig. 8(a) reveals that, within the dark stripe area, the O atom distribution is enhanced and the value is almost constant. Namely, the asymmetric shape of the O distribution is a result of the increase in the number of the O atoms distributed in the light-stripe area along the propagation direction, shown by yellow lines in Fig. 8(d). On the other hand, in the small wave structure, comparing the O distribution in Fig. 9(d) with the optical microscope image in Fig. 9(a), it is found that the asymmetric shape is formed by decreasing the number of the O atoms distributed in the light-stripe area along the propagation direction of the small wave structure [yellow lines in Fig. 9(d)]. In the complex labyrinthine structure, as shown in Figs. 10(a) and 10(d), the asymmetric shape of O distribution [Fig. 10(d)] is also created by the increase in the number of the O atoms distributed in the light-stripe area toward the propagation direction of the pattern [yellow lines in Fig. 10(d)]. Such spatial asymmetric shapes depending on the propagation direction of the pattern are very similar to the spatial distribution shape of the chemical concentration of the chemical traveling wave in the reaction-diffusion system, the shape of which is due to the reaction decay of the chemicals. The chemical traveling wave forms a periodic asymmetric shape by the sloping of the reacting chemical concentration toward the propagation of the wave. The shape similarity indicates that these spatiotemporal patterns might be formed by the chemical wave. However, the fact that the slope direction of the small wave structure (opposite that of the propagation) is opposite that of the chemical traveling wave (toward the propagation) indicates that the small wave structure might not be a mere chemical wave in the reaction-diffusion system. The propagation direction for the small wave structure might be controlled by another factor except for the chemical reaction, for example, the natural convection which generally emerges on the electrode surface during electrodeposition [23–25] as mentioned above, even if the small wave structure is the chemical wave.

C. Relationship between O atoms and dynamic property of pattern

In order to clarify the role of O, element analysis was implemented for the electrodeposited films, which are uniformly black and white on the electrode surface. The uniformly black and white films with no spatiotemporal patterns were formed by electrodeposition in the ranges of current density lower and higher than the range in which the three spatiotemporal patterns emerge, respectively. The results of the element analysis are shown in Table VI. The area with a diameter of 200 μm was measured. The result indicates that the O atomic percents ($\sim$4 at. %) of the uniformly white and black films are much lower than the average O atomic percents of the three patterns, from $\sim$8 to $\sim$11 at. % (from Tables I, III, and V) although the atomic percents of the other light elements, C, S, and K, are nearly the same. Moreover, the local element analysis of the only uniformly black film was carried out because it has a convexo-concave part on the surface while the uniformly white film has no convexo-concave part [18]. The black film has upheaving grains on the μm order accumulating on the surface. The experiment was carried out for two parts, the upheaving part and the other flat part in the black film, in the measurement area with a diameter of 1 μm. The results for the two parts in the black film are also shown in Table VI. The results show that the Ag and Sb atomic percents in the upheaving part are 94 and 0.52 at. %, respectively, while the Ag and Sb atomic percents in the other flat part are 70 and 13 at. %. Namely, the difference in the atomic percent indicates that two parts of the metal composition in the black film exist as in the dark- and light-stripe areas in the three spatiotemporal patterns. However, the upheaving grains in the black film do not move on the electrode surface, differing from the three spatiotemporal patterns. This difference in movement might be caused by the amount of O, and the higher amount of O might be related to the dynamic property of the patterns as mentioned above.

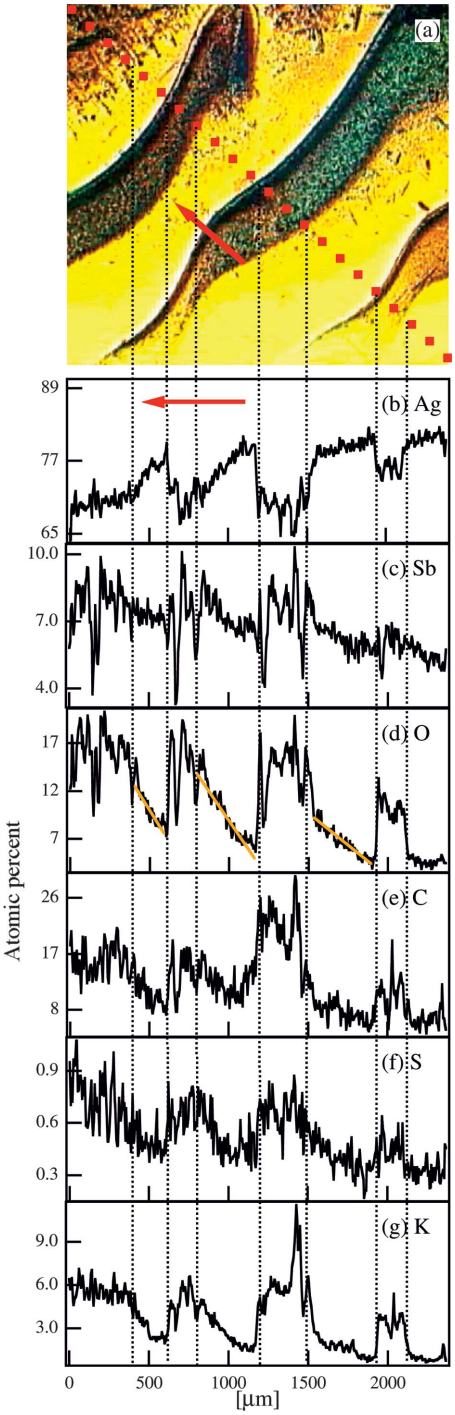

FIG. 8. (Color) Optical microscope image of area of big wave structure investigated in element map analysis [(a)] and element distributions on a line corresponding to the red broken line drawn on (a), in respective element maps of Figs. 3(b)–3(g) [(b) Ag distribution, (c) Sb distribution, (d) O distribution, (e) C distribution, (f) S distribution, and (g) K distribution]. The respective element distributions are averaged with a width of 20 pixels in the element maps. The red arrows in (a) and (b) indicate the propagation direction of the big wave structure. The black dotted lines are drawn for the crossing points of the red broken line and the boundary line of the light- and dark-stripe areas in (a). The yellow lines in (d) indicate the slope of O atom distribution in the light-stripe area.

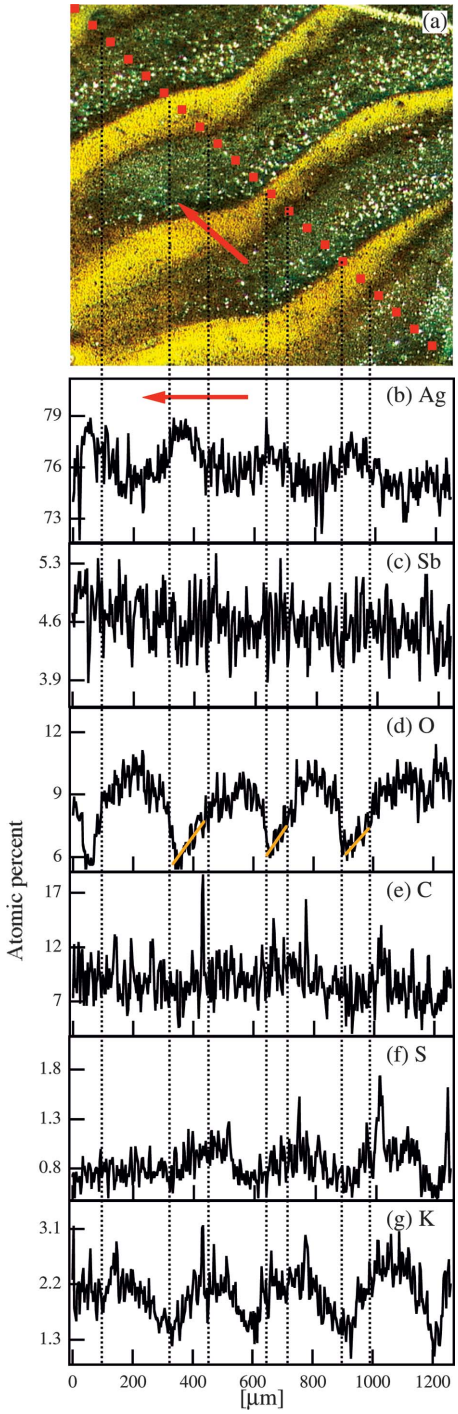

FIG. 9. (Color) Optical microscope image of area of small wave structure carried out in element map analysis [(a)] and element distributions on line corresponding to the red broken line drawn in (a), in respective element maps of Figs. 5(b)–5(g) [(b) Ag distribution, (c) Sb distribution, (d) O distribution, (e) C distribution, (f) S distribution, and (g) K distribution]. The respective element distributions are averaged with a width of 20 pixels in the element maps. The red arrows in (a) and (b) indicate the propagation direction of the small wave structure. The black dotted lines are drawn for the crossing points of the red broken line and the boundary line of the light- and dark-stripe areas in (a). The yellow lines in (d) indicate the slope of O atom distribution in the light-stripe area.

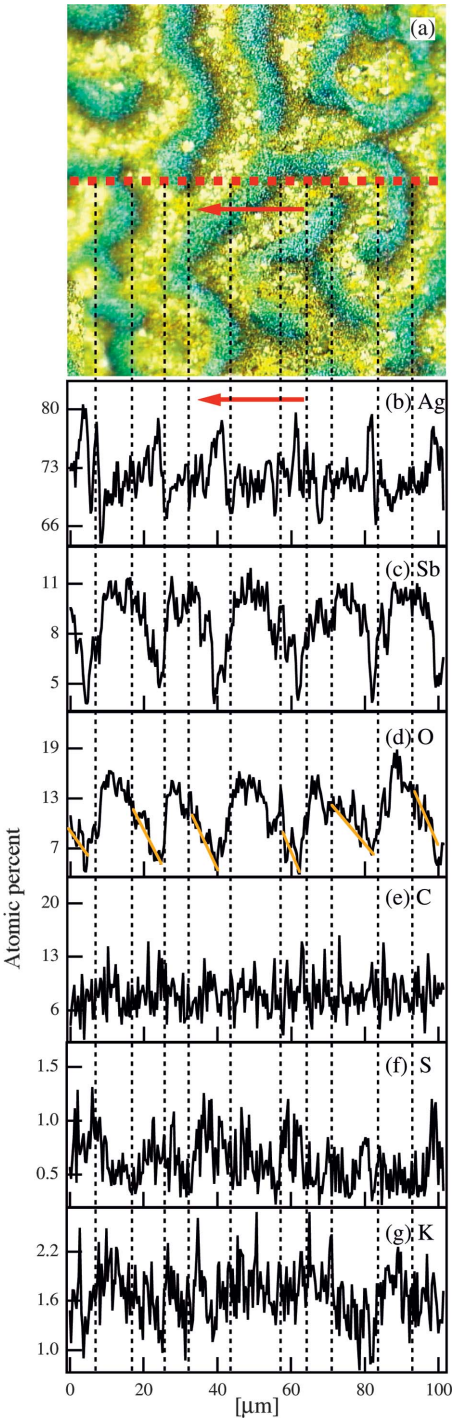

FIG. 10. (Color) Optical microscope image of area of complex labyrinthine structure investigated in element map analysis [(a)] and element distributions on a line corresponding to the red broken line drawn in (a), in respective element maps of Figs. 7(b)–7(g) [(b) Ag distribution, (c) Sb distribution, (d) O distribution, (e) C distribution, (f) S distribution, and (g) K distribution]. The respective element distributions are averaged with a width of 20 pixels in the element maps. The red arrows in (a) and (b) indicate the propagation direction of the complex labyrinthine structure. The black dotted lines are drawn for the crossing points of the red line and the boundary line of the light- and dark-stripe areas in (a). The yellow lines in (d) indicate the slope of O atom distribution in the light-stripe area.

Furthermore, the fact that O atomic percents in these spatiotemporal stripe patterns are higher than that in the uniformly black and white electrodeposited surface with no spatiotemporal pattern suggests that O atom emergence in spatiotemporal patterns cannot be ascribed to only the oxidation after drying in air and is intrinsic to the spatiotemporal stripe patterns.

D. Different element ratios in different patterns

The big wave structure analyzed in Fig. 3 is formed in the area after the big wave structure destroys the complex labyrinthine structure which had been formed on the electrode surface before the big wave structure surged. Namely, the big wave structure and the complex labyrinthine structure investigated in Figs. 3 and 7 are within the same phase in the phase diagram as functions of the constant current density (~ -11 mA/cm^2) applied to the electrodes during electrodeposition [16]. Generally, the total amount of electrodeposited components is determined by and is proportional to the constant current density. However, the ratio of Ag atomic percent to Sb atomic percent for the big wave structure is considerably different from that for the complex labyrinthine structure; they are 11 and 8.1, respectively, which are calculated from the average atomic percents of Ag and Sb for the entire area of the Ag and Sb maps shown in Tables I and V. Namely, the total electrodeposited amount, which the constant current density contributes to, remains the same while the ratio of the components is significantly changed depending on the type of pattern. This implies that the difference in the ratio of Ag atomic percent to Sb atomic percent might be due to the difference in the concentrations of the chemical components of the solution near the electrode surface. Actually, the fact that potential changes with pattern change during the electrodeposition, which was reported in a previous paper [17], also supports the change in the solution concentration on the electrode surface. This component difference in the vicinity of the electrode surface might be caused by the emergence of natural convection in the vicinity of the electrode surface [23–25], to which the pattern formation of the big wave structure is considered to be strongly ascribed, as mentioned above.

Furthermore, the ratio of Ag atomic percent to Sb atomic percent in any areas of the three spatiotemporal patterns is higher than that of typical alloys, $Ag_{0.84}Sb_{0.16}$ and $Ag_{3.15}Sb_{0.85}$ [26,27], and the ratios of Ag atomic percent to Sb atomic percent in all the light and dark stripes of the three spatiotemporal stripe patterns also show that they are all richer in Ag than typical alloys. Therefore it is suggested that they are formed by the solid solubility of Sb in Ag.

V. CONCLUSIONS

Element analysis by EPMA was implemented for three spatiotemporal stripe patterns by Ag and Sb coelectrodeposition. These patterns have already been specified in terms of stripe wavelength and stripe velocity in our previous papers. The element analysis results indicate that all patterns are composed of the six elements, Ag, Sb, O, C, S, and K. Fur-

TABLE VI. Element atomic percents for uniformly white and black electrodeposited films detected in a measurement area of 200 μm diameter and element atomic percents for an upheaving part and an other flat part in a uniformly black electrodeposited film, which are locally investigated in a measurement area with a diameter of 1 μm.

	Uniform white (at. %)	Uniform black (at. %)	Upheaving part in uniform black (at. %)	Flat part in uniform black (at. %)
Ag	87	81	94	70
Sb	1.2	6.7	0.52	13
O	4.6	4.1	2.6	5.7
C	8.7	7.6	8.4	7.0
S	0.76	0.59	0.87	0.33
K	1.1	0.55	0.42	0.68

thermore, the element map analysis reveals that the common distributions in all patterns are that more Ag atoms are contained in the light-stripe area than in the dark-stripe area and more Sb, O, and K atoms tend to be contained in the dark-stripe area than in the light-stripe area. More O atoms than Sb atoms are contained in all patterns and, in addition, the difference between light- and dark-stripe areas in O atomic percent is larger than that in Sb atomic percent. The results indicate that O is also important in the pattern formation, as well as Ag and Sb, which have been advocated so far. As a model for the origin of O, the oxidation of Sb was proposed and an electrochemical reaction formula for the oxidation was suggested.

ACKNOWLEDGMENTS

We thank T. Watanabe of the advanced development and supporting center in RIKEN for support and for allowing us use of the EPMA. This work was partially supported by a Grant-in-Aid for Scientific Research (Y.N.) from the Ministry of Education, Culture, Sports, Science and Technology in Japan.

[1] A. N. Zaikin and A. M. Zhabotinsky, Nature (London) **225**, 535 (1970).
[2] C. Sachs, M. Hildebrand, S. Völkening, J. Wintterlin, and G. Ertl, Science **293**, 1635 (2001).
[3] D. Walgraef, in *Spatio-Temporal Pattern Formation* (Springer, New York, 1996).
[4] C. Bowman and A. C. Newell, Rev. Mod. Phys. **70**, 289 (1998).
[5] O. Steinbock, T. Ágota, and K. Showalter, Science **267**, 868 (1995).
[6] M. Assenheimer and V. Steinberg, Nature (London) **367**, 345 (1994).
[7] Y. Hu, R. Ecke, and G. Ahlers, Phys. Rev. E **48**, 4399 (1993).
[8] E. Bodenschatz, W. Pesch, and G. Ahlers, Annu. Rev. Fluid Mech. **32**, 709 (2000).
[9] *Ordered and Turbulent Patterns in Taylor-Couette Flow*, edited by C. D. Andereck and F. Hayot (Plenum, New York, 1992).
[10] S. Kai, N. Chizumi, and M. Kohno, Phys. Rev. A **40**, 6554 (1990).
[11] M. Seul, L. R. Monar, L. O. Gorman, and R. Wolfe, Science **254**, 1616 (1991).
[12] Y. Li, J. Oslonovitch, N. Mazouz, F. Plenge, K. Krischer, and G. Ertl, Science **291**, 2395 (2001).
[13] M. Kim, M. Bertram, M. Pollmann, A. von Oertzen, A. S. Mikhailov, H. H. Rotermund, and G. Ertl, Science **292**, 1357 (2001).
[14] I. Krastev and M. T. M. Koper, Physica A **213**, 199 (1995).
[15] I. Krastev, M. Nikolova, and I. Nakada, Electrochim. Acta **34**, 1219 (1989).
[16] Y. Nagamine and M. Hara, Physica A **327**, 249 (2003).
[17] Y. Nagamine, N. Kurono, and M. Hara, Thin Solid Films **460**, 87 (2004).
[18] Y. Nagamine, O. Haruta, and M. Hara, Surf. Sci. **575**, 17 (2005).
[19] M. Bertram, C. Beta, H. H. Rotermund, and G. Ertl, J. Phys. Chem. B **107**, 9610 (2003).
[20] A. L. Lin, M. Bertram, K. Martinez, H. L. Swinney, A. Ardelea, and G. F. Carey, Phys. Rev. Lett. **84**, 4240 (2000).
[21] *Electrodeposition of Metals and Alloys*, edited by N. E. Khomutov (Israel Program for Scientific Translations, Jerusalem, 1969), p. 11.
[22] K. Krischer, in *Modern Aspects of Electrochemistry, Number 32*, edited by B. E. Conway *et al.* (Kluwer Academic/Plenum, New York, 1999), p. 10.
[23] F. Alavyoon, Electrochim. Acta **37**, 333 (1992).
[24] C. B. Shin and J. D. J. Economou, J. Electrochem. Soc. **138**, 527 (1991).
[25] S. Nakabayashi, I. Krastev, R. Aogaki, and K. Inokuma, Chem. Phys. Lett. **294**, 204 (1998).
[26] W. H. King and B. T. Massalski, Philos. Mag. **6**, 669 (1961).
[27] D. J. Scott, Can. Mineral. **14**, 139 (1976).